Journal of Hazardous Materials 192 (2011) 1491–1504

Contents lists available at ScienceDirect

Journal of Hazardous Materials

journal homepage: www.elsevier.com/locate/jhazmat

Sulphur mustard degradation on zirconium doped Ti–Fe oxides

Václav Štengl[a,*], Tomáš Matys Grygar[a], František Opluštil[b], Tomáš Němec[b]

[a] Department of Solid State Chemistry, Institute of Inorganic Chemistry AS CR v.v.i 250 68 Husinec-Řež, Czech Republic
[b] Military Technical Institute of Protection Brno Veslařská 230, 628 00 Brno, Czech Republic

ARTICLE INFO

Article history:
Received 14 April 2011
Received in revised form 23 June 2011
Accepted 25 June 2011
Available online 1 July 2011

Keywords:
Warfare agents
Nanodispersive oxides
Homogeneous hydrolysis
Urea

ABSTRACT

Zirconium doped mixed nanodispersive oxides of Ti and Fe were prepared by homogeneous hydrolysis of sulphate salts with urea in aqueous solutions. Synthesized nanodispersive metal oxide hydroxides were characterised as the Brunauer–Emmett–Teller (BET) surface area and Barrett–Joiner–Halenda porosity (BJH), X-ray diffraction (XRD), infrared (IR) spectroscopy, scanning electron microscopy (SEM) with energy-dispersive X-ray (EDX) microanalysis, and acid–base titration. These oxides were taken for an experimental evaluation of their reactivity with sulphur mustard (chemical warfare agent HD or bis(2-chloroethyl)sulphide). The presence of Zr^{4+} dopant tends to increase both the surface area and the surface hydroxylation of the resulting doped oxides in such a manner that it can contribute to enabling the substrate adsorption at the oxide surface and thus accelerate the rate of degradation of warfare agents. The addition of Zr^{4+} to the hydrolysis of ferric sulphate with urea shifts the reaction route and promotes formation of goethite at the expense of ferrihydrite. We discovered that Zr^{4+} doped oxo-hydroxides of Ti and Fe exhibit a higher degradation activity towards sulphur mustard than any other yet reported reactive sorbents. The reaction rate constant of the slower parallel reaction of the most efficient reactive sorbents is increased with the increasing amount of surface base sites.

1. Introduction

Due to the increased threat of chemical attacks by terrorist organizations, there is renewed interest in the environmental fate of chemical warfare agents (CWAs), including blister agents such as sulphur mustard (HD or bis(2-chloroethyl)sulphide) and lewisite (usually found as a mixture, of 2-chlorovinylarsonous dichloride as well as bis(2-chlorovinyl)arsinous chloride–"lewisite 2" and tris(2-chlorovinyl) arsine–"lewisite 3"), and nerve agents such as tabun (GA or ethyl N,N-dimethylphosphoramidocyanidate), sarin (GB or O-isopropyl methylphosphonofluoridate), soman (GD or 3,3-dimethylbutan-2-yl methylphosphonofluoridate), and VX (ethyl ({2-[bis(propan-2-yl)amino]ethyl}sulfanyl)(methyl)phosphinate) [1].

Knowledge of processes that influence the fate and transport of CWAs in the environment can aid in predictions of environmental persistence, estimates of exposure, and the development of decontamination and disposal strategies. Because CWAs are highly toxic and their use is restricted in non-surety laboratories, research on the environmental fate of CWAs is often conducted using simulant compounds (less toxic chemical analogs). A variety of compounds have been used as simulants for HD, such as 2-chloroethyl methyl sulphide (CEMS), 2-chloroethyl phenyl sulphide (CEPS), chloroethyl ethyl sulphide (CEES), also called half-mustard (HM) and methyl salicylate (MS) [2].

A number of potential simulants for GA, GB, and GD have been identified – diphenyl chlorophosphate (DPCP), dimethyl methylphosphonate (DMMP), diethyl ethylphosphonate (DEEPT), triethylphosphate (TEP) and diisopropyl methylphosphonate (DIMP). Amiton or tetram (VG, O,O-diethyl-S-[2-(diethylamino)ethyl] phosphorothioate) is a "V-series" nerve agent and is commonly used to simulate the VX agent. Additional compounds have been used to simulate VX include O,S-diethyl phenylphosphonothioate (DEPP) and organophosphorus pesticides, such as malathion and parathion (E605).

In the late 1990s, reactive sorbents based on metal oxides (Ca, Mg, and Al) were proposed to CWA degradation [3–6] instead of soluble chemical agents and carbon [7] the most traditional and till now used practically in military decontamination routines. Further progress in this direction has been achieved during the last several years with transition metal oxides. The results of the work [8] show that dimethyl methylphosphonate (DMMP), a simulant for P-containing CWA agents, can be oxidatively decomposed over Au nanoparticles supported on TiO_2. The thermal decomposition of

* Corresponding author. Tel.: +420 2 6617 3534; fax: +420 2 2094 0157.
E-mail address: stengl@iic.cas.cz (V. Štengl).

0304-3894/$ – see front matter © 2011 Elsevier B.V. All rights reserved.
doi:10.1016/j.jhazmat.2011.06.069

dimethyl methylphosphonate (DMMP) on high surface area TiO_2 nanoparticles (Degussa P25) has been studied [9] by transmission infrared spectroscopy. Nanocrystalline zinc(II) oxide materials were prepared by a sol–gel method with an average crystallite size ~55 nm of zincite phase. Obtained materials were tested as destructive adsorbents for the decontamination of sarin with a rate constant and the half-life to be 4.12 h^{-1} and 0.16 h, respectively in the initial stages of the reaction and 0.361 h^{-1} and 1.9 h at the final stages of the reaction for the decontamination reaction on nanocrystalline ZnO [10].

Detoxification reactions of sulphur mustard (HD), the chemical warfare agent, were studied on the surface of zinc oxide nanorods at room temperature (32 ± 2°C) and the data were compared with that of bulk ZnO. The data explored the role of hydrolysis and elimination reactions in the detoxification of sulphur mustard and it also revealed that zinc oxide nanorods and bulk ZnO showed the half-life of 8.48 h, 24.75 h in the first 12 h and 122.47 h, 177.29 h from 12 h to 48 h of the reaction [11].

Mixed metal oxide nanocrystals of AP-Al_2O3, AP-Al_2O_3–Fe_2O_3, AP-Al_2O_3–V_2O_5 and AP-Al_2O_3–CuO were prepared by the aerogel process. One hundred percent of sulphur mustard was found to be decontaminated on Al_2O_3–Fe_2 O_3, Al_2O_3–V_2O_5 and Al_2O_3–CuO where only 75% of the same was found to be decontaminated on AP-Al_2O_3 within 40 h [12]. Reactions of sulphur mustard and sarin were decontaminated on $V_{1.02}O_{2.98}$ nanotubes [13]. Nanocrystalline zinc oxide materials were prepared by the sol–gel method. Sarin was hydrolysed to form a surface bound non-toxic phosphonate on the surface of nano zinc oxide. The data also revealed the values of rate constant and half-life to be 4.12 h^{-1} and 0.16 h in the initial stages of the reaction and 0.361 h^{-1} and 1.9 h at the final stages of the reaction for the decontamination reaction on nanocrystalline ZnO [10,14]. Mesoporous manganese oxides nanobelts were synthesized by the hydrothermal-ion exchange method, decontamination reaction exhibited a pseudo first-order behaviour and the values of rate constant and half-life were found to be 0.43 h^{-1} and 1.6 h for sarin (GB), 0.01 h^{-1} and 61.32 h for sulphur mustard (HD) and 0.02 h^{-1} and 34.66 h for chloroethyl ethyl sulphide (CEES) [15]. Manganese(III,IV) oxides were prepared by a homogeneous hydrolysis of potassium permanganate with 2-chloroacetamide and direct reaction of potassium permanganate with manganese(II) sulphate in aqueous solutions [16]. The degree of conversion for sulphur mustard and agent VX is very good for both prepared samples and come up to 95% and 99%, respectively, after 64 min. In contrast to sulphur mustard and agent VX, degradation of soman was only 56% of the cryptomelane-type MnO_2 and 18% of the birnessite-type MnO_2. In comparison with published results [17] where rate constant k = 0.01 h^{-1} for the soman degradation on manganese oxide nanotubes and nanosheets was given, manganese(III,IV) oxides prepared by Štengl et al. [16] allows a reaction rate by several orders of magnitude faster. Modified titania nanotubes have been studied as powder decontaminants against sulphur mustard (HD). Decontamination reactions were carried out at room temperature (30 ± 2 ° C) and monitored by gas chromatography and gas chromatography mass spectrometry techniques [18].

The homogeneous hydrolysis mixture of titanium oxo-sulphate and zirconium oxo-sulphate with urea at a temperature of 100 °C was used to prepare Zr^{4+} doped anatase with a high specific surface area [19]. The structure and photocatalytic activity of Zr doped titania nanocrystallites with a varying Zr content between 0 and 15 wt% prepared by an efficient and environmentally benign method was studied by vibrational spectroscopy, TEM and XRD [20]. All titania samples up to 13 wt% Zr doping concentration showed better or similar photoreactivity compared to P25 (Degussa) for the decomposition of adsorbed 2-chloroethyl ethyl sulphide (CEES) and dimethyl methylphosphonate (DMMP) in synthetic air at room temperature. Zirconium doped nanodispersive oxides of Fe, Al and Zn were prepared by homogeneous hydrolysis of sulphate salts with urea in aqueous solutions. These oxides were taken as an experimental evaluation of their reactivity with sulphur mustard, soman and a VX agent [21].

The reactive sorptive decay of CWAs on metal oxide reactive sorbents is a fast method of their removal by both immobilisation and decay. Because sorption and hydrolysis are the principal reactions, surface acid and base functional groups ($^{\bullet}O$, $^{\bullet}OH$, $^{\bullet}OH_2$) are expected to be the driving force of the reaction. A large specific surface area of reactive sorbents is a prerequisite for the fast immobilising CWAs, but the chemical quality of the surface is expected to guarantee the chemisorption (irreversibility of immobilisation) and later chemical decomposition. The acid–base titrations were hence chosen to characterise the "chemical quality" of the surface of the reactive sorbents.

The aim of this work was to evaluate the performance of a series of nanocrystalline Fe–Ti oxides modified with minor amounts of Zr in the removal of the HD warfare agent (further denoted only by its empirical nam, sulphur mustard) from its solution using similar experimental conditions, as in our previous studies [19,21]. In the present study, a Zr^{4+} doped mixture of nanodispersive titanium and iron oxides were directly synthesized by homogeneous hydrolysis from aqueous solutions [22]. Solutions of titanium oxo-sulphate, iron sulphate and zirconium oxo-sulphate were heated with urea and nanometre-sized particles agglomerated in spherical clusters were obtained. Their reactivity with sulphur mustard was examined. Principle factors controlling the activity of reactive sorbents and their further optimisation were found.

2. Experimental

2.1. Preparation of samples

All chemical reagents used in the present experiments were obtained from commercial sources and were used without further purification. HD (sulphur mustard, bis(2-chloroethyl) sulphide), purity 91.2%, was obtained from an approved laboratory governed by the Slovak Ministry of Defence. $TiOSO_4$, $Fe_2(SO_4)_3$, $ZrCl_4$ and urea were supplied by Fluka (Munich, Germany). $ZrOSO_4$ was prepared by a reaction of stoichiometric amount of $ZrCl_4$ and sulphuric acid. $ZrCl_4$ was dissolved in a 98% sulphuric acid solution in a porcelain crystallisation dish, heated at 100 °C until HCl escaped from the reaction mixture. Then the solution was heated to crystallisation; the product identity was verified by X-ray powder diffraction ($ZrOSO_4$, ICDD PDF card No. 01-0366).

The Zr^{4+} doped mixed Ti and Fe oxides were prepared by homogeneous hydrolysis of $TiOSO_4$ and $Fe_2(SO_4)_3$ with $ZrOSO_4$ in aqueous solutions using urea as the precipitation agent. In a typical process, $TiOSO_4$ and $Fe_2(SO_4)_3$ were dissolved in 100 mL of hot distilled water acidified with 98% H_2SO_4. The pellucid liquid was diluted into 4 L of distilled water, a defined amount of $ZrOSO_4$ was added (see Table 1) and the solution was mixed with 400 g of urea. The mixture was heated at 100 °C for 9 h under stirring until pH reached 7.2; at this pH gaseous ammonia is released from the solution. The formed precipitates were decanted, filtered and dried at 105 °C. Twenty eight samples (seven series, each with four samples) of mixed nanodispersive Fe–Ti–Zr oxides were prepared in like manner (Table 1). The prepared samples were denoted as Ti*XX*Fe*YY*Zr*Z*, where *XX*, *YY* and *Z* are input masses of titanium, iron, and zirconium salts.

2.2. Characterisation methods

X-ray diffraction (XRD) patterns were obtained by a Siemens D5005 instrument using Cu Kα radiation (40 kV, 30 mA) and

Table 1
Reaction conditions, phase composition, crystallite size, surface area and porosity of prepared samples.

Sample	$TiOSO_4$ [g]	$ZrOSO_4$ [g]	$Fe_2(SO_4)_3$ [g]	EDX Zr [wt%]	Anatase content [%]	Anatase Crystallite size [nm]	Goethite content [%]	Goethite Crystallite size [nm]	Surface area BET [m^2g^{-1}]	Total pore volume [cm^3g^{-1}]	Micropore surface area [m^2g^{-1}]	Micropore volume [cm^3g^{-1}]
Ti05Fe95Zr_1	5	1	95	1.01	0	–	100	6.6	248.8	0.2253	26.075	0.0097
Ti05Fe95Zr_2	5	2	95	2.09	0	–	100	4.5	668.2	0.5216	118.19	0.0471
Ti05Fe95Zr_3	5	3	95	3.01	0	–	100	4.2	206.4	0.2951	0	0
Ti05Fe95Zr_4	5	5	95	5.28	0	–	100	4.2	220.3	0.2677	0	0
Ti10Fe90Zr_1	10	1	90	1.1	0	–	100	10.4	358.7	0.4776	0	0
Ti10Fe90Zr_2	10	2	90	2.56	0	–	100	9.5	344.6	0.4829	7.53	0.00142
Ti10Fe90Zr_3	10	3	90	3.25	0	–	100	6.4	356.4	0.3873	26.80	0.01029
Ti10Fe90Zr_4	10	5	90	4.87	0	–	100	6.3	459.3	0.5695	3.59	0.00068
Ti25Fe75Zr_1	25	1	75	1.11	0	–	100	7.8	405.7	0.4974	0	0
Ti25Fe75Zr_2	25	2	75	3.73	0	–	100	7.6	490.7	0.6516	0	0
Ti25Fe75Zr_3	25	3	75	5.11	0	–	100	7.2	625.6	0.8280	0	0
Ti25Fe75Zr_4	25	5	75	7.24	0	–	100	6.2	832.9	0.9866	0	0
Ti50Fe50Zr_1	50	1	50	1.23	71.2	4.4	28.8	6.6	520.5	0.5750	0	0
Ti50Fe50Zr_2	50	2	50	3.11	62.3	3.3	37.7	6.4	582.3	0.5810	0	0
Ti50Fe50Zr_3	50	3	50	5.22	53.1	3.4	46.9	6.2	565.3	0.5619	0	0
Ti50Fe50Zr_4	50	5	50	6.89	59	1.7	41.0	5.1	495.0	0.5370	0	0
Ti75Fe25Zr_1	75	1	25	1.15	100	5.2	0	–	595.8	0.4843	0	0
Ti75Fe25Zr_2	75	2	25	2.56	100	4.4	0	–	628.6	0.4916	0	0
Ti75Fe25Zr_3	75	3	25	4.11	100	3.7	0	–	628.4	0.5090	0	0
Ti75Fe25Zr_4	75	5	25	6.98	100	3.6	0	–	752.4	0.6190	0	0
Ti90Fe10Zr_1	90	1	10	1.05	100	6.4	0	–	462.3	0.4017	0	0
Ti90Fe10Zr_2	90	2	10	2.98	100	6.5	0	–	522.3	0.4541	0	0
Ti90Fe10Zr_3	90	3	10	4.72	100	6.2	0	–	422.3	0.4311	0	0
Ti90Fe10Zr_4	90	5	10	6.24	100	5.8	0	–	535.9	0.4277	0	0
Ti95Fe05Zr_1	95	1	5	2.01	100	6.9	0	–	511.1	0.4371	0	0
Ti95Fe05Zr_2	95	2	5	3.76	100	6.5	0	–	562.2	0.5007	0	0
Ti95Fe05Zr_3	95	3	5	8.1	100	6.4	0	–	578.5	0.4700	0	0
Ti95Fe05Zr_4	95	5	5	9.41	100	6.4	0	–	436.3	0.3170	64.16	0.0252

diffracted beam monochromator. Data were collected in a step-scan mode covering angles from 5° to 90°. Qualitative analysis was performed with the Eva Application and the X'Pert HighScore using the JCPDS PDF-2 database [23] and crystallite sizes were determined using Rietveld refinement of the XRD spectra with Bruker TOPAS v.4.0 software and with structural models based on an ICSD database [24]. The surface area of the samples degassed for 15 min at 150 °C was determined from nitrogen adsorption–desorption isotherms at a liquid nitrogen temperature using a Coulter SA3100 instrument. Langmuir BET method was used for surface area calculation [25], while pore size distribution (pore diameter and volume) was determined by the BJH method [26].

Scanning electron microscopy (SEM) studies were performed using a Philips XL30 CP microscope equipped with energy dispersive X-ray (EDX) fluorescence spectral analysis for element composition and Robinson secondary electron (SE) and back-scattered electron (BSE) detectors for imaging. The sample was placed on an adhesive carbon slice and coated with Au–Pd alloy 10 nm thick layer.

Infrared spectra were recorded by using a Thermo-Nicolet Nexus 670 FT-IR spectrometer in 4000–500 cm^{-1} and 500–50 cm^{-1} regions, respectively, with a single-reflection horizontal accessory on Si crystal. The samples were pressed into KBr pellets in ambient conditions and measured in the transmission mode.

Acid–base titration was performed after suspending 2 g of a sorbent in 20 mL water. Initial pH of the aqueous suspension was measured, and then it was titrated by either HCl, or NaOH solutions using a combined glass pH electrode. The results of the titrations were expressed in mmol of HCl or NaOH per gram of sorbent to reach the pH values of the suspension 3 or 9, respectively.

2.3. Method of warfare agents degradation

Synthesized powdery samples were dried for 24 h at 100 °C and 400 Pa before tests. A weighed portion of the dry samples was put into a glass vial provided with a screw solid cap (Supelco, type CRS-33). Sulphur mustard was dosed onto a layer of the evaluated solid in the form of a nonane solution (6% w/v). 150 μL of that solution was pipetted onto 50 mg of the solid reagent which resulted in dosage of 1 mg of the toxic agent per 50 mg of the evaluated solid. The vial was sealed with a cap and put into a constant temperature vessel. All experiments were performed at 25 °C, and each run was repeated four to six times. Adding 2 propanol (1.85 mL) terminated the reaction. The solid reagent was immediately separated from suspension by centrifugation (5 000 r.p.m. for 5 min). Aliquots of the resulting supernatant were analysed for residual contents of sulphur mustard by GC/FPD using an Agilent Technologies gas chromatograph 6890 N with FPD-P and FPD-S detectors.

3. Results

3.1. Characterisation of the composition

In Fig. 1, the selected XRD patterns of the nanodispersive oxides Ti–Fe–Zr prepared from $TiOSO_4$ and $Fe_2(SO_4)_3$ doped with $ZrOSO_4$ are presented. Anatase (ICDD PDF, card No. 21-1272) is dominant in samples with higher contents of Ti (Fig. 1a–c), while goethite FeO(OH) (ICDD PDF, card No. 29-0713) prevails in samples with a higher content of Fe (Fig. 1e–f). The reaction of ferric sulphate with urea usually leads to pure ferrihydrite $Fe_5O_7(OH)\cdot 4H_2O$ [27], however, the presence of Zr favours a goethite formation, which is in agreement with our previous study of Fe–Zr system [21]. In the ternary metal oxide systems, zirconium occurs either incorporated/occluded in Fe and Ti oxides or in other forms not detectable by XRD as a distinct phase. The calculated crystallite sizes of prepared samples are presented in Table 1. By increasing Zr content at a given Fe/Ti ratio, crystallite sizes of goethite and anatase decrease. That effect was attributed to a complex compound $[Zr(OH)_n]^{4-n}$ formed during the hydrolysis, which prevents the formation of crystalline particles and supports the formation of gels and amorphous phases [28]. That effect was also reported for zirconium doped titania [19] and zirconium doped nanodispersive Fe, Al and Zn oxides [21].

Fig. 2 infrared spectra presents nanodispersive mixed oxides Ti–Fe–Zr with varying proportions of titanium, iron and zirconium. Bands of O–H of the water group are visible in all spectra. Vibration bands for ν(O–H) groups on the oxide surfaces resonate in 3400 cm^{-1}. The band 1630 cm^{-1} is a part of the deformation vibration of OH group of water. The bands at 1400 cm^{-1} and 880 cm^{-1} (see Fig. 2a–f) are associated with the vibration of CO_3^{2-} group (tabulated fundamental vibration of infrared spectrum are ν_3 = 1415 cm^{-1} and ν_2 = 880 cm^{-1}). Many bands in the area around 1100 cm^{-1} prove the presence of sulphates in the sample (see Fig. 2a, e and f). SO_4^{2-} groups have tabulated fundamental vibrations ν_3 at 1104 cm^{-1} and ν_4 at 611 cm^{-1}. Sulphate coordination to metal ions lowers the symmetry of the SO_4^{2-} groups and consequently increases some spectral bands, and it also activates the vibration ν_1 981 cm^{-1} [29]. These two vibrations, ν_4 and ν_1, partially obscure vibrations of the Ti–O bond expected to produce bands below 600 cm^{-1}. The presence of the Zr oxide has not been proven, perhaps because the band of Zr–O for monoclinic lattice at 745, 625, 530, 450 and 490 cm^{-1} for a cubic lattice has very broad bands [30]. Vibrations of the Fe–O bond appear with the increasing proportion of Fe in the samples, frequencies of which vary according to the polymorph. Two bands, at 898 and 796 cm^{-1} (see Fig. 2e and f), indicate the presence of goethite α-FeO(OH) [29].

Table 1 presents the specific surface area (BET), total pore volume, micropore surface area and micropore volume related to the porosity of prepared zirconium doped Fe–Ti oxides. The Barrett–Joyner–Halenda (BJH) pore-size distribution plot and nitrogen adsorption/desorption isotherms (inset) of prepared zirconium doped Ti–Fe oxides are shown in Fig. 3.

According to the International Union of Pure and Applied Chemists (IUPAC) notation [31], microporous materials have pore diameters of less than 2 nm and macroporous materials greater than 50 nm; the mesoporous category thus lies within this interval. Samples with higher Ti content have the type I isotherm, characteristic for microporous powders, pore size of which does not exceed a few diameters of adsorbate molecules. The size of pores for these samples is close to micropores, corresponding to size of 2–3 nm. The type II isotherm, characteristic for solid with pores larger then micropores, was actually obtained with samples with a higher Fe content. The size of mesopores have maximum of 3–5 nm. In addition, the samples Ti10Fe90Zr_2–Ti10Fe90Zr_4 have a micropore surface area from 3 $m^2\ g^{-1}$ to 27 $m^2\ g^{-1}$, samples Ti05Fe95Zr_1 and Ti05Fe95Zr_2 have a micropore surface area 26 $m^2\ g^{-1}$ and 118 $m^2\ g^{-1}$ and finally the sample Ti95Fe05Zr_4 have a micropore surface area 64 $m^2\ g^{-1}$.

At a relative pressure above 0.3, de Boer [32] identified five types of hysteresis loops, which he attributed to various pore shapes. For all studied samples, the type A hysteresis was observed, and hence is attributable to cylindrical pores open at both ends. In samples with increasing Zr content, the proportion of mesopores decreases and the specific surface area increases. All samples are characterised by large specific surface areas, namely, Ti75Fe25Zr_4 and Ti25Fe75Zr_4 have 752 $m^2\ g^{-1}$ and 833 $m^2\ g^{-1}$, respectively, which is comparable with materials prepared using a more technologically demanding supercritical drying method called aerogels [6,33–35].

Fig. 4 is a representative SEM micrograph of the prepared Ti–Fe–Zr nanodispersive oxides. The samples consist of spherical

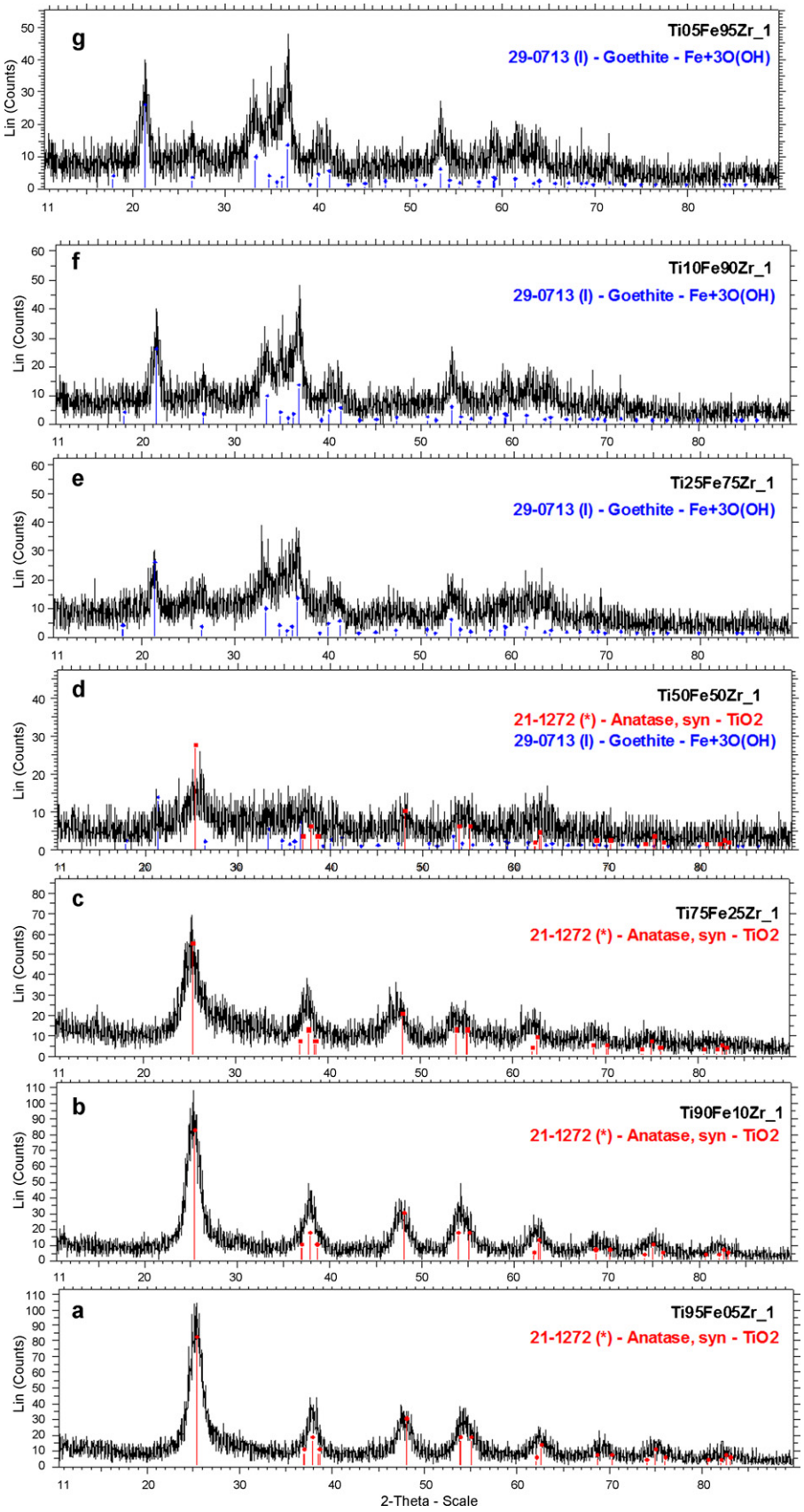

Fig. 1. XRD patterns of the samples nanodispersive oxides (a) Ti95Fe05Zr_1, (b) Ti90Fe10Zr_1, (c) Ti75Fe25Zr_1, (d) Ti50Fe50Zr_1, (e) Ti25Fe75Zr_1, (f) Ti10Fe90Zr_1, (g) Ti05Fe95Zr_1.

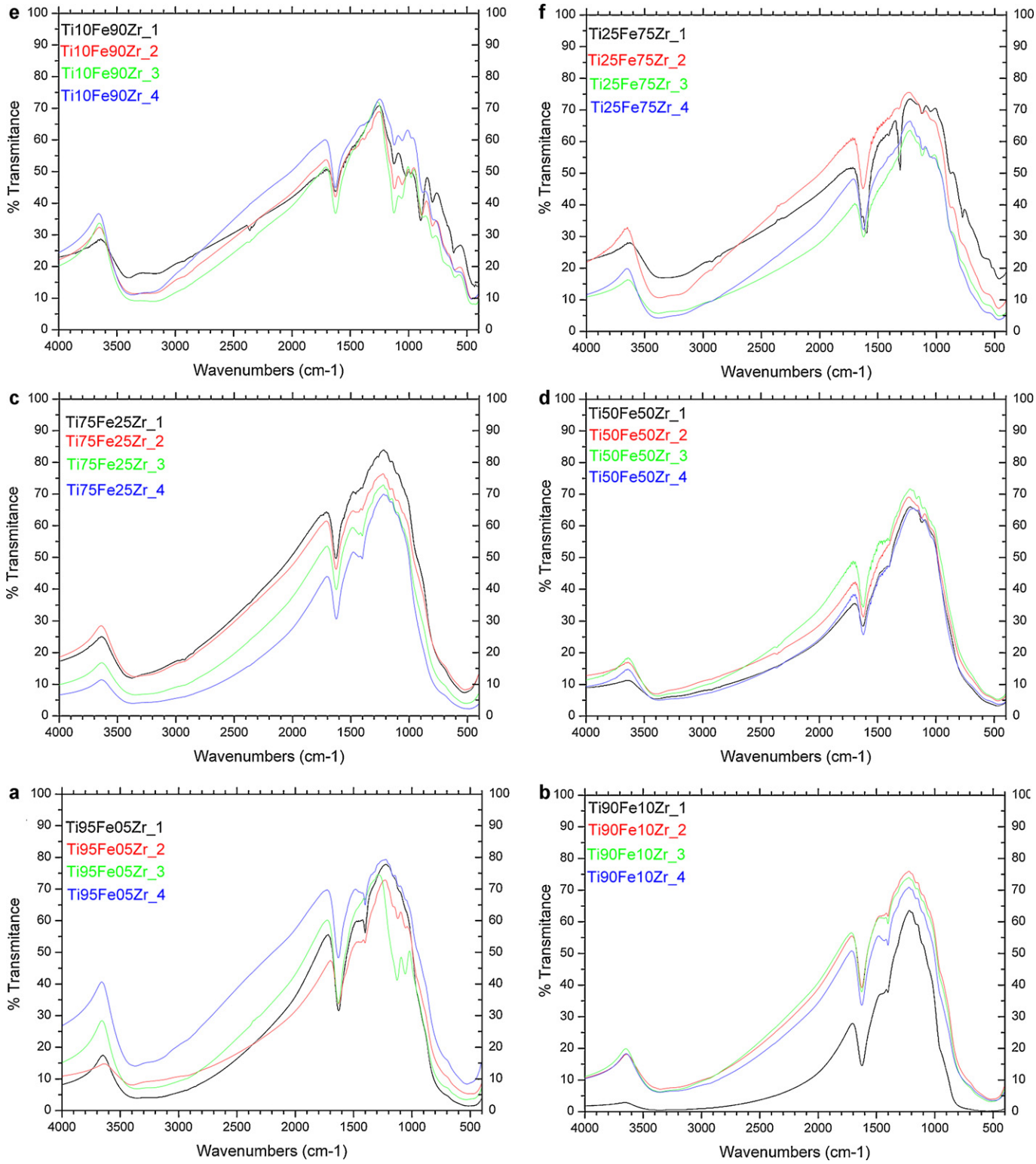

Fig. 2. Infrared spectra of series samples (a) Ti95Fe05Zr, (b) Ti90Fe10Zr, (c) Ti75Fe25Zr, (d) Ti50Fe50Zr, (e) Ti10Fe90Zr, (f) Ti25Fe75Zr.

agglomerates of size 1–2 μm; samples with a higher Fe content (Fig. 4e and f) have a clearly visible mesoporous texture. EDX produced analyses of the actual contents of Zr in prepared samples (Table 1). Fig. 5 shows an image of a typical TiO_2 nanocrystal. Viewing high-resolution TEM interconnected structures that form a porous material arranged with numerous little corners and edges. The metal cations are white spots and oxygen ions are the black spots. Cationic sites (M^+) inside the crystal (not shown) have a coordination number 6; cations in the surface (labelled 1 in Fig. 5) have a coordination number 5; cations at the edges (labelled 2) have a coordination number 4, and cations in corners (labelled 3) have a coordination number 3. The surface defect gap reduces the

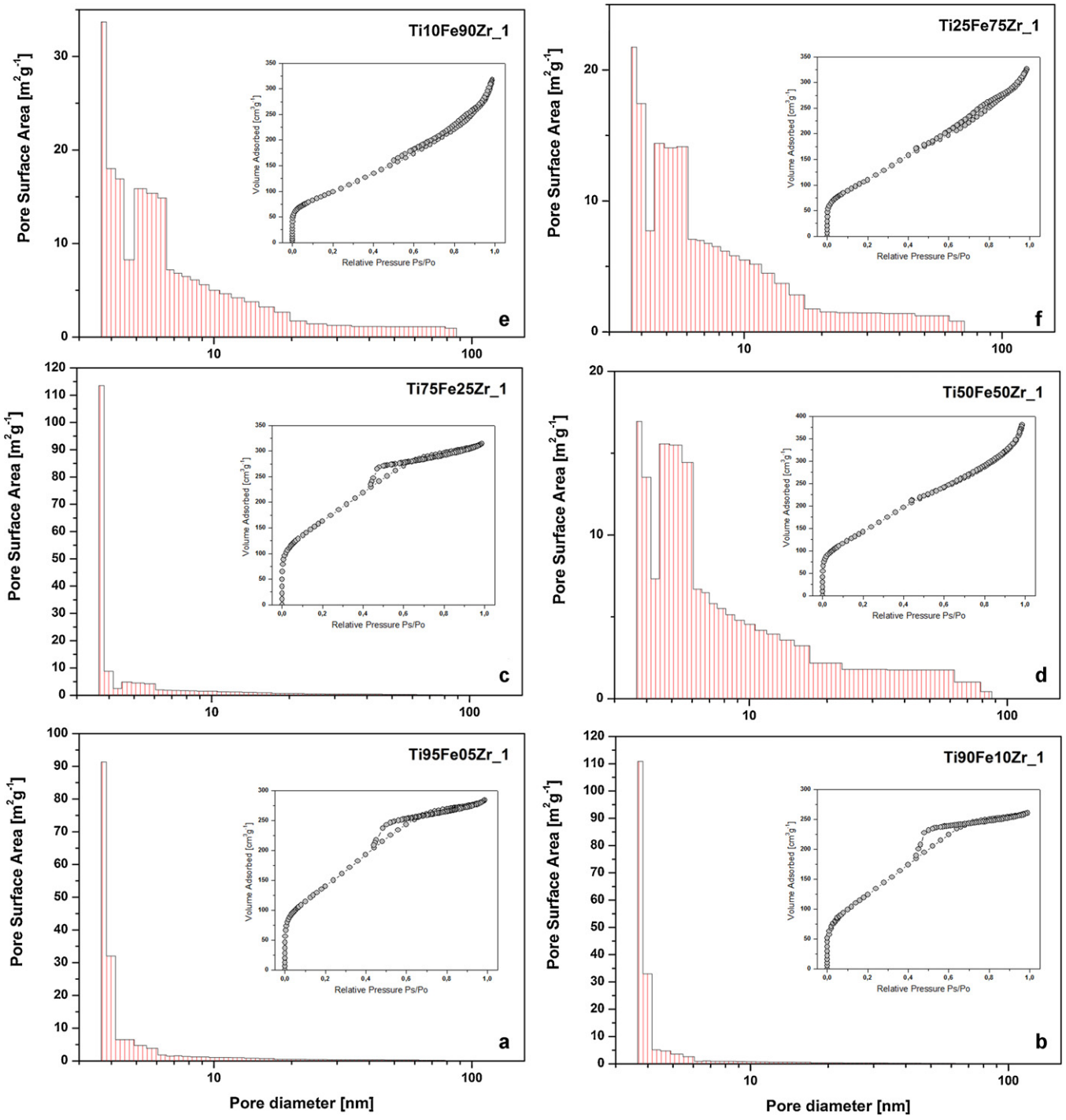

Fig. 3. Pore surfaces are distribution plot and nitrogen adsorption/desorption isotherms (inset) of samples (a) Ti95Fe05Zr_1, (b) Ti10Fe90Zr_1, (c) Ti75Fe25Zr_1, (d) Ti50Fe50Zr_1, (e) Ti10Fe90Zr_1, (f) Ti25Fe75Zr_1.

coordination number of surrounding ions (arrows 4). The lower the coordination number of cations, the higher their reactivity.

3.2. Kinetics of sulphur mustard removal

The degradation of CWAs including sulphur mustard with ternary Ti–Fe–Zr oxides proceeds in two stages [36]. For the formal kinetic description, an equation with two fitted rate constants has been approved:

$$q_\tau = q_1 \exp(-k_1 \tau) + q_2 \exp(-k_2 \tau) + q_\infty \quad (1)$$

where q_τ represents residual quantity of the toxic agent in a time τ, q_1 and q_2 are the fractions of more or less active parts of the surface nanodispersive material, respectively, k_1 and k_2 are rate constants of corresponding stages (sub-processes or steps), q_∞ is the residual amount of toxic agent at the end of the reaction, if the destructive capacity of powdery reagent has not been sufficient to complete it. In the performed experiments, q_∞ was below 0.3%. The fits of experimental data using Eq. (1) are shown in Figs. 6 and 7 and the refined rate constants k_1 and k_2 and degree of conversion at the end of the experiment are listed in Table 2. The relationship between k_1 and k_2 and degree of conversion is shown in Fig. 8b and c.

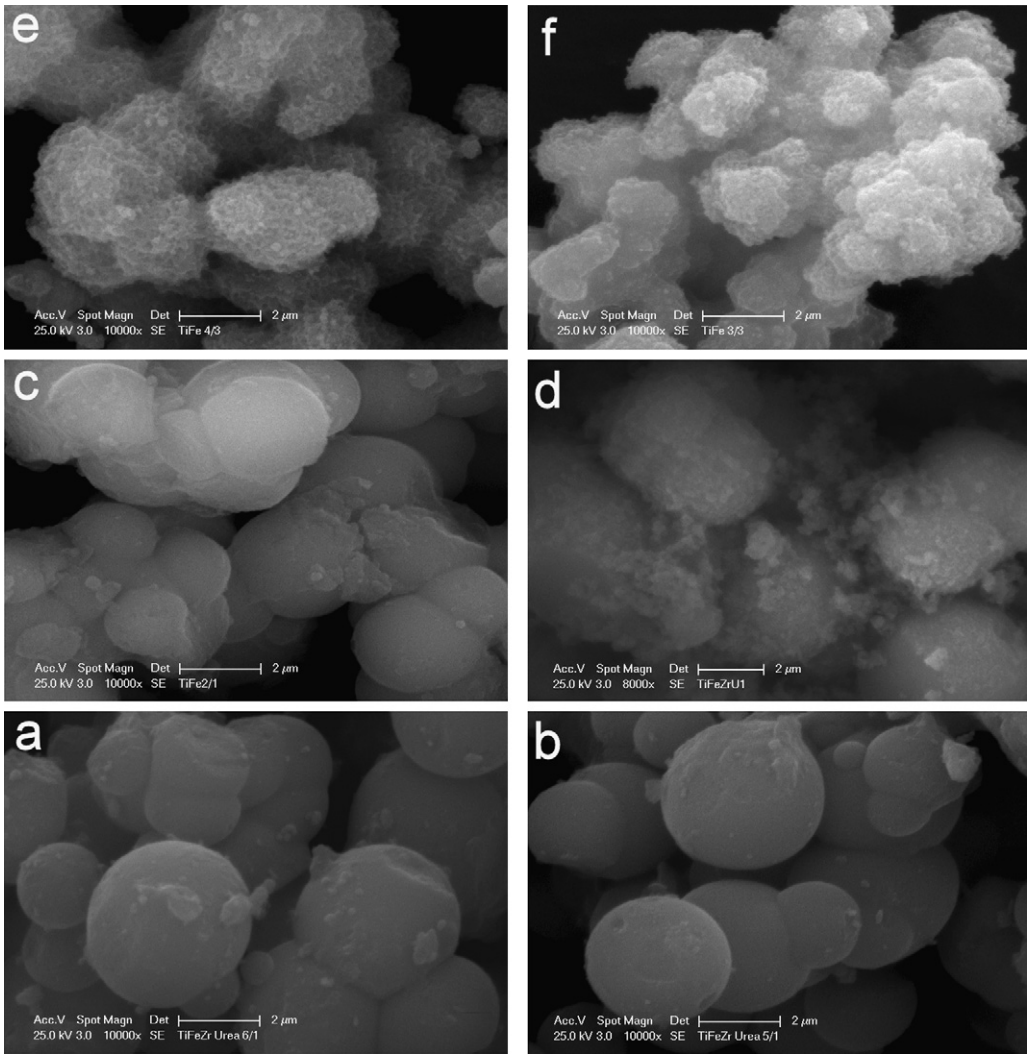

Fig. 4. SEM micrograph of (a) Ti95Fe05Zr_1, (b) Ti10Fe90Zr_1, (c) Ti75Fe25Zr_1, (d) Ti50Fe50Zr_1, (e) Ti25Fe75Zr_3, (f) Ti10Fe90Zr_3.

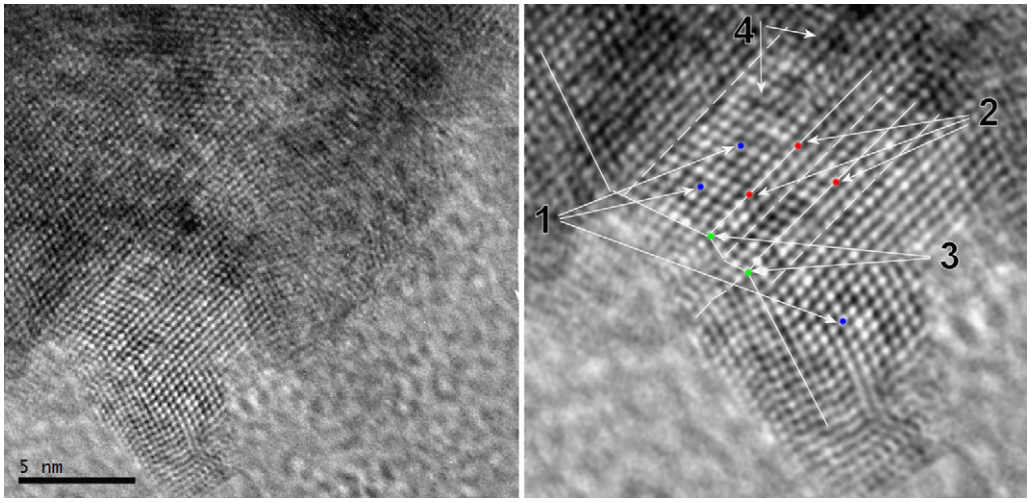

Fig. 5. High-resolution TEM interconnected structures of titania nanocrystal. Cations in the surface (labelled 1) have a coordination number 5, cations at the edges (labelled 2) have coordination number 4, and cations in corners (labelled 3) have coordination number 3. Surface defect gap reduces the coordination number of surrounding ions (arrows 4).

Table 2
Degree of conversion, rate constat k_1 and k_2 and results of acido–basic titrations.

Sample	Degree of conversion [%]	Rate constant k_1 [s^{-1}]	Rate constant k_2 [s^{-1}]	HCl consumtion to reach pH = 3 [mmol g^{-1}]	NaOH consumtion to reach pH = 3 [mmol g^{-1}]	pH of aquous suspension
Ti05Fe95Zr_1	95.69	4.39E−02	4.55E−04	0	1.42	1.86
Ti05Fe95Zr_2	96.01	2.87E−02	5.01E−04	0	1.76	1.56
Ti05Fe95Zr_3	93.63	2.63E−02	5.19E−04	0.11	0.41	5.05
Ti05Fe95Zr_4	94.79	1.36E−02	4.95E−04	0.09	0.59	4.36
Ti10Fe90Zr_1	95.66	1.30E−02	5.56E−04	0.01	0.58	3.00
Ti10Fe90Zr_2	97.79	1.71E−02	6.84E−04	0.01	0.60	3.10
Ti10Fe90Zr_3	95.99	2.48E−02	5.35E−04	0	0.98	2.47
Ti10Fe90Zr_4	98.09	1.28E−02	7.51E−04	0.03	0.37	4.31
Ti25Fe75Zr_1	94.98	1.11E−02	5.41E−04	0.09	0.33	4.62
Ti25Fe75Zr_2	95.89	9.21E−03	5.77E−04	0.10	0.32	6.04
Ti25Fe75Zr_3	97.68	1.85E−02	9.25E−04	0.04	0.36	4.63
Ti25Fe75Zr_4	96.31	5.17E−03	6.50E−04	0.26	0.14	6.76
Ti50Fe50Zr_1	98.55	3.23E−02	9.79E−04	0.12	0.46	5.49
Ti50Fe50Zr_2	99.48	4.48E−02	9.94E−04	0.04	0.48	4.09
Ti50Fe50Zr_3	98.52	3.20E−02	4.30E−04	0.19	0.42	6.50
Ti50Fe50Zr_4	99.35	3.52E−02	9.44E−04	0.11	0.42	6.13
Ti75Fe25Zr_1	99.02	4.01E−02	1.30E−03	0.28	0.37	7.37
Ti75Fe25Zr_2	99.48	3.02E−02	9.73E−04	0.24	0.38	6.87
Ti75Fe25Zr_3	99.07	3.78E−02	1.47E−03	0.34	0.40	7.19
Ti25Fe75Zr_4	98.49	3.36E−02	1.20E−03	0.34	0.46	6.99
Ti90Fe10Zr_1	89.22	3.04E−03	2.44E−04	0.27	0.28	7.48
Ti90Fe10Zr_2	93.15	1.05E−02	5.07E−04	0.24	0.30	7.33
Ti90Fe10Zr_3	96.35	7.34E−03	6.02E−04	0.26	0.34	7.70
Ti90Fe10Zr_4	97.09	9.03E−03	6.76E−04	0.30	0.36	7.22
Ti95Fe05Zr_1	98.47	6.73E−02	1.81E−03	0.33	0.29	7.61
Ti95Fe05Zr_2	97.47	1.09E−02	6.46E−04	0.27	0.42	6.28
Ti95Fe05Zr_3	99.08	1.32E−02	1.16E−03	0.36	0.31	7.49
Ti95Fe05Zr_4	98.46	3.02E−02	1.06E−03	0	1.28	2.01

4. Discussion

4.1. Comparison of Fe–Ti–Zr oxides and other reactive sorbents

The prepared Ti–Fe–Zr samples reach a high degree of conversion after 64 min (95–98%) and some of the newly synthesized and tested ternary compositions are more efficient than binary Zr doped FeOOH [21] and Zr doped titania [19]. According to the chemical analyses by GC/FPD, sulphur mustard is decomposed on the surface of Zr^{4+} doped mixture of nanodispersive titania and iron oxides to non-toxic products [36] similar to other transition oxides ([37] and references therein). The idea of reactive sorption of CWAs, i.e., sorption accompanied by chemical decay, instead of mere sorption by carbonaceous materials, was first verified using a high-surface area alumin [3,38] and about a decade ago "aerogels", fluffy nanodispersive MgO and alumina [4,39]; the decay was attributed to hydrolysis on the surface OH and H_2O functionalities. During recent years, transition-metal oxides have been shown to be superior to alumina and aerogels [6]. Transition metal oxides offer a very broad scale of materials to be tested. Some of them also invoke further reaction mechanisms of the CWAs degradation: photocatalysis with respect to titania [40,41] or oxidation regarding Mn(III,IV) oxides [15,16,42], but this report only deals with non-photocatalytic and non-oxidative decomposition. In this reaction, some of Fe–Ti–Zr oxides seem to be the best materials but still reported in terms of kinetics of CWAs removal. A study of them was invoked by the extraordinarily good performance of Zr-doped titania [21] and Zr doped Fe oxides [19]. To perform the comparison of results achieved thus far with other reactive sorbents, actual experimental setup and some kinetics considerations are essential.

The reaction kinetics of sulphur mustard decomposition on ternary Fe–Ti–Zr oxides involves two steps, of which the first is fast (expressed as k_1 in the used kinetic model of two parallel reactions, Eq. (1)) and the second is slower by several orders of magnitude (k_2). The second process is crucial for total conversion (Fig. 8c); whenever it is smaller than $9 \times 10^{-4}\ s^{-1}$, the resulting conversion after 64 min cannot be larger than 98.6%. The rate of the first process is not so critical (Fig. 8b), although conversions after 64 min cannot be over 98% whenever k_1 is lower than $1 \times 10^{-2}\ s^{-1}$. In previous analogous experiment set-ups for CWAs removal by reactive sorbents, only one exponential member and one constant k member from Eq. (1) was sufficient for the formal reaction kinetics [19]. Also in reports by other researchers, a single exponential decay was used for fitting kinetic curves [43,44]. Typical rate coefficients so obtained were about $3 \times 10^{-5}\ s^{-1}$ for mustard gas removal by alumina aerogel [44], which roughly corresponded to k_2 listed in Table 2 and/or k listed in Table 3. Contrarily, the rate constants k_1 obtained with ternary Fe–Ti–Zr oxides (Tables 2 and 3) as well as single rate constants k reported previously for binary systems of Zr-doped Ti oxides and Zr-doped Fe oxides [19,21] are on the order of 10^{-3} to $10^{-2}\ s^{-1}$, indicating a substantially faster reaction. We can suppose that k_1 rate constant corresponds to a certain reaction specific to Fe and Ti oxides, which does not proceed with Mg and Al oxides. To better specify this fast reaction, we checked the influence of the specific surface area and also surface acid–base sites obtained by acid–base titration, similar to Tang et al. [37], who used a temperature programmed desorption of NH_3 or CO_2 (TPD) for comparing reactive sorbents with a very divergent element and phase composition.

Neither the reaction conversion (see Fig. 8a) nor the two partial rate constants (Fig. 9) of the studied set of Fe–Ti–Zr oxides are simply related only to the samples' specific surface area that points to the importance of the variability of the surface functional groups somehow related to a different element and/or phase composition of the sorbents. The element/phase composition is obviously the most important factor of the phenomenological description of reaction kinetics and individual chemical parameters of the catalysts, as was concluded also by Winter et al. [45]. The fact that the specific surface area is by no means the most relevant factor controlling the reaction kinetics is clear from the wide range of

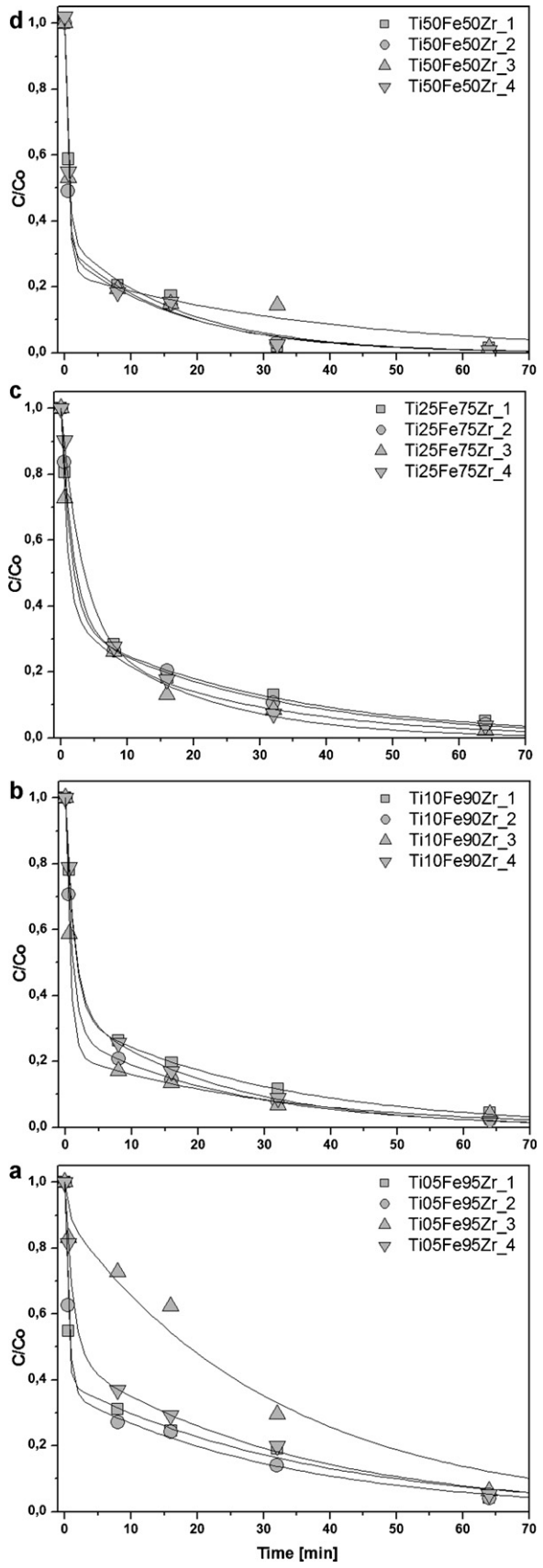

Fig. 6. The plots of degradations of sulphur mustard on samples series (a) Ti05Fe95Zr, (b) Ti10Fe90Zr, (c) Ti25Fe75Zr and (d) Ti50Fe50Zr.

Table 3
Comparison of hydroxy-oxides with best performance to mustard gas decomposition. The removal of toxic agent has been performed under comparable .experiment setups.

Sample	Preparation	Degree of conversion after 64 min [%]	$\tau_{1/2} = \ln 2/k$ or $\tau_{1/2} = \ln 2/k_1 \times \ln 2/k_2$ [min]	k [s^{-1}]	k_1 [s^{-1}]	k_2 [s^{-1}]	Reference
MgO	Aerogel	68.0	23.1	5×10^{-4}	–	–	[35]
Al oxide	Aerogel	–	385	3×10^{-5}	–	–	[44]
Al oxide	Aerogel	–	1200	–	–	–	[11]
Modified Al oxide	Aerogel, impregnated by Keggin anions	–	231–385	$(3–5)\times10^{-5}$	–	–	[43]
TiO_2 anatase	Urea hydrolysis	96.5	3.7	3.1×10^{-3}	–	–	[27]
Zn doped anatase	Urea hydrolysis	98.7	3.5	3.3×10^{-3}	–	–	[47]
Zr doped[a] anatase	Urea hydrolysis	96.0	0.6	–	1.4×10^{-1}	$2–6\times10^{-3}$	[19]
In doped anatase	Urea hydrolysis	98.5	8.5	–	2.2×10^{-2}	7.1×10^{-4}	[48]
Ge doped anatase	Urea hydrolysis	97.7	0.6	–	1.9×10^{-1}	1.2×10^{-3}	[49]
ferrihydrite	Urea hydrolysis	83.5	4.5	2.5×10^{-3}	–	–	[27]
Fe–Zr oxides	Urea hydrolysis	95.0	2.26	5.1×10^{-3}	–	–	[21]
Al–Zr oxides	Urea hydrolysis	74.0	6.1	1.9×10^{-3}	–	–	[21]
Zn–Zr oxides	Urea hydrolysis	47.7	13.1	8.9×10^{-4}	–	–	[21]
MnO_2 cryptomelane type	Chloroacetamide hydrolysis	95.1	2.7	–	1.4×10^{-2}	3.5×10^{-3}	[49]
MnO_2 birnessite type	Chloroacetamide hydrolysis	95,8	5.0	2.3×10^{-3}	–	–	[49]
TiO_2–MnO_2	Chloroacetamide hydrolysis	95.2	1.3	–	4.7×10^{-2}	2.1×10^{-3}	[49]
Mn substituted ammonium–jarosite	Chloroacetamide hydrolysis	95,5	13.1	–	2.6×10^{-2}	3.9×10^{-4}	[49]
Fe substituted MnO_2	Chloroacetamide hydrolysis	97,8	0,5	–	1,36	1.5×10^{-3}	[49]

[a] Degree of conversion 32 min.

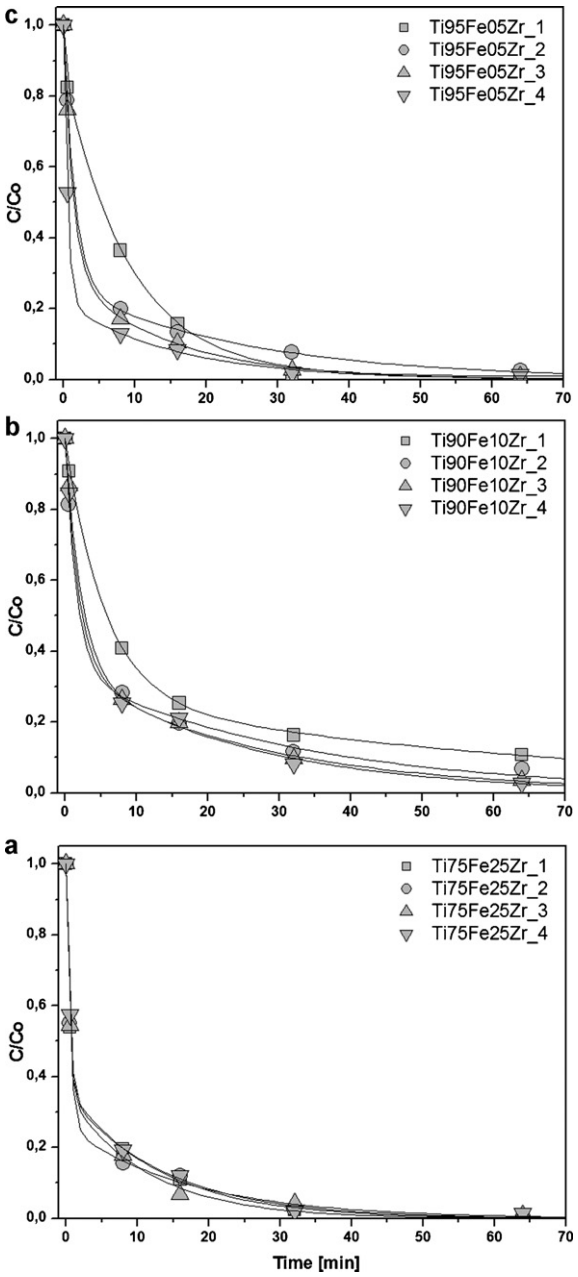

Fig. 7. The plots of degradations of sulphur mustard on samples series (a) Ti75Fe25Zr, (b) Ti90Fe10Zr and (c) Ti95Fe05Zr.

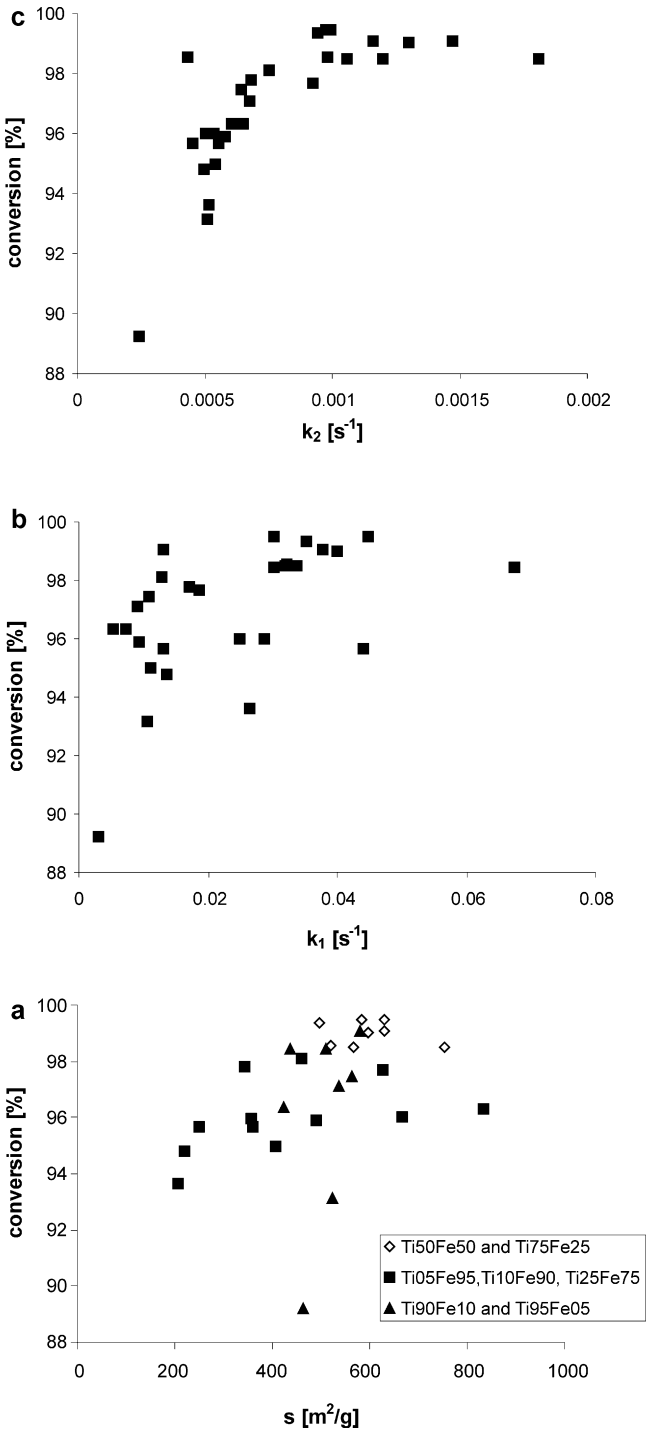

Fig. 8. The dependence of reaction conversion after 64 min on a specific surface area and the two individual components k_1 and k_2 for the entire set of reactive sorbents.

conversions achieved after 64 min with samples with the specific surface area in the range 400–600 $m^2\ g^{-1}$ (Fig. 8a). The specific features of the Fe–Ti–Zr oxide catalysts for the three groups of their composition are listed below to decipher the factors controlling their performance.

4.2. Behaviour of goethite rich sorbents (Ti05Fe9–Ti25Fe75)

The performance of these Zr-modified goethites is worse than most anatase containing specimens although still much better than most of the known non-titania reactive sorbents (Tables 2 and 3). The rate constant of the first step, k1 of these samples is not dependent on the specific surface area of the specimens. On the other hand, it is increased when the sorbents have low pH of aqueous suspension and correspondingly high NaOH consumption to reach pH 9 (Fig. 10a), a reaction step obviously enhanced by acid functional groups. The rate constant k_2 of the second step is increased only minimally with a growing specific surface area (Fig. 9b), i.e., it is not directly proportional to it, and so its increase itself cannot improve the performance very much. That constant slightly increases with the increasing pH of aqueous suspension of the sorbents and decreases with NaOH consumption to reach pH 9 (Fig. 10a); it is noteworthy that this effect is opposite to that of k_1. Perhaps this contradiction contributes to the lower final reaction conversion for which both k_1 and k_2 should be as large as possible.

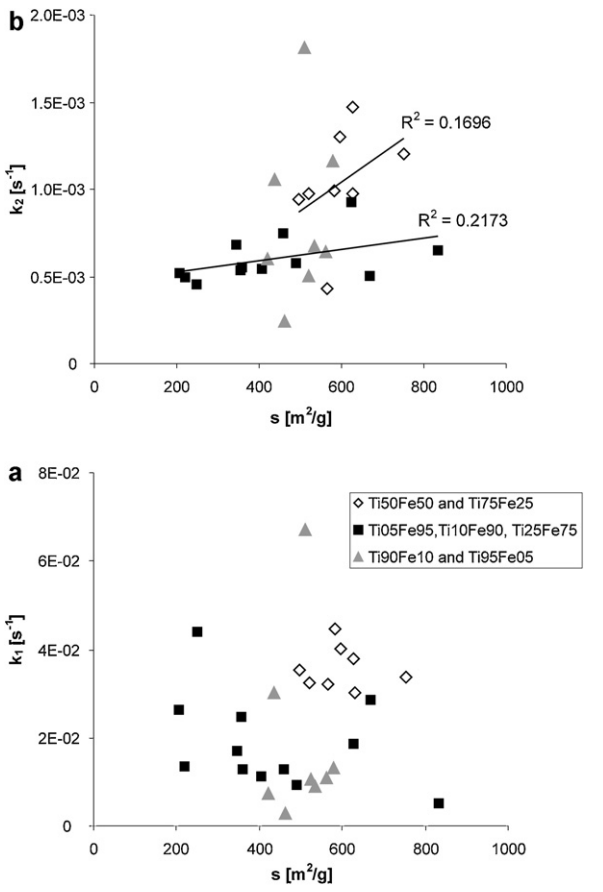

Fig. 9. The dependence of the kinetic components k_1 and k_2 on the specific surface area for three groups of reactive sorbents according to their element and phase composition.

Optimisation of these catalysts by varying their surface acid–base properties could hardly be possible.

4.3. Behaviour of anatase sorbents with moderate Fe contents (Ti50Fe50, Ti75Fe25)

The best results (i.e., the fastest sulphur mustard removal, the highest conversions after 64 min) have been obtained with oxides containing comparable amounts of Fe and Ti. In terms of phase composition they were a mixture of nanocrystalline goethite and anatase (Ti50 series) or only anatase (Ti75 series). According to XRD analysis, the anatase components in these mixtures have smaller crystallite sizes than in anatase compositions with a smaller Fe content (discussed in the next section). The rate constant of the first process, k_1, is largest from the entire data set and seems independent of the specific surface area (Fig. 9a). The constant k_1 weak growth with the increasing HCl consumption to reach pH 3 and pH of aqueous suspension of the catalysts (Fig. 10c). The rate constant of the second reaction step, k_2, is proportional to the specific surface area (Fig. 9b) and is also dependent on the acid–base properties of the catalysts. The samples with the highest pH of aqueous suspension have both large k_1 and k_2; obviously the base groups are favourable to both of the reaction steps.

4.4. Behaviour of anatase sorbents with low Fe content (Ti90Fe10, Ti95Fe05)

This group of sorbents is very heterogeneous as for their performance; however, there are no statistically significant correlations between k_1 and k_2 on the one hand and specific surface area (Fig. 9a)

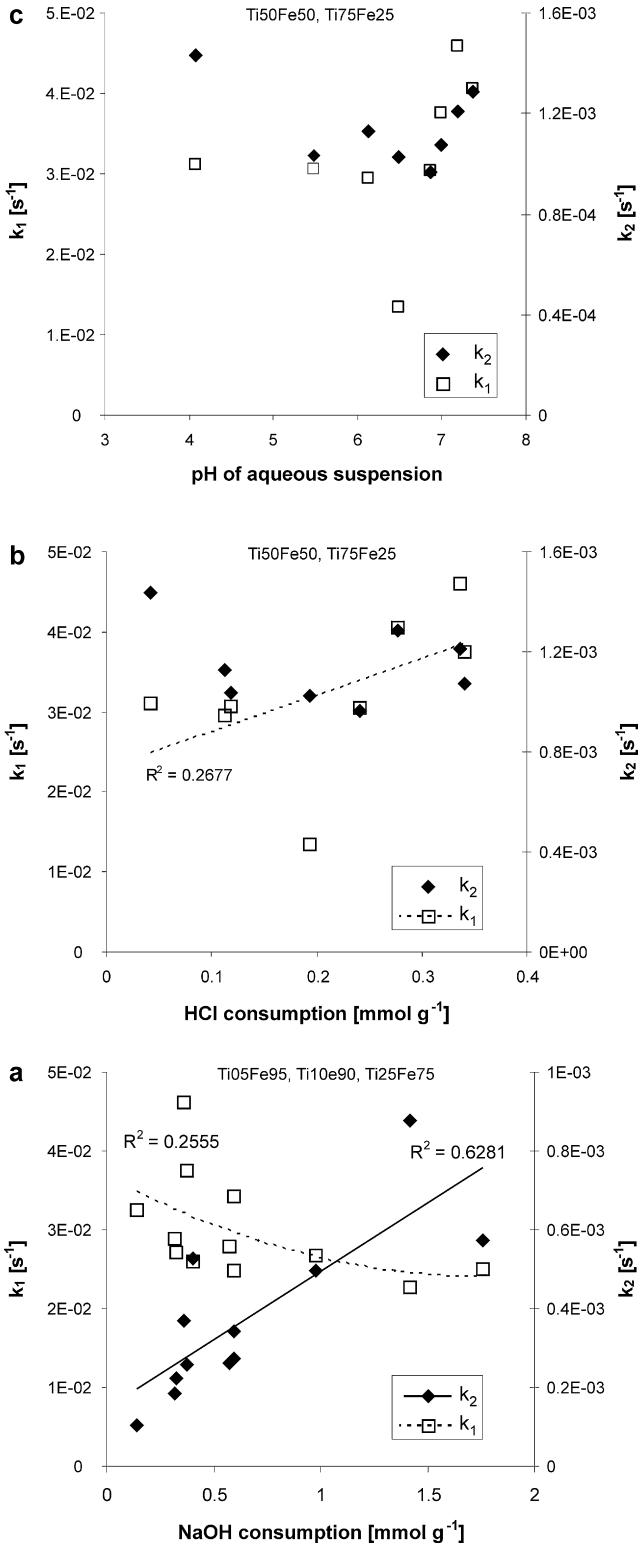

Fig. 10. The relationships between kinetic components k_1 and k_2 and the acid base properties for selected reactive sorbents. (a) Dependence of goethite rich sorbents on NaOH consumptions to reach pH 9, (b) dependence of anatase sorbents with moderate Fe content on HCl consumption to reach pH 3, and (c) the dependence of the same sorbents on pH of aqueous suspensions.

and acid–base properties on the other. Most of the specimens had comparably poor efficiency with the goethite-rich ones, except for three catalysts with the highest content of Ti. Most catalysts of this group have k_1 close to or lower than 1×10^{-2} s^{-1} which is not sufficient for getting high conversions. However, the experimental data set does not propose a phenomenological description of the reaction kinetics and instead proposes a factor which could explain their better performance.

4.5. Overall evaluation of Fe–Ti–Zr reactive sorbents

In the experiment setup used in this study, the specific surface areas of the sorbents are not really critical for the total reaction conversion under the chosen w/w ratio of sulphur mustard and the solid as these values do not correlate; it is confirmed also by q_∞ on the order of 10^{-1} percent. Whenever surface areas are too low with respect to the amount of CW, final conversions on the order of a few tens percent are common, such as in large-particle size metal oxides shown by Winter et al. [45].

The very fast reaction pathway characterised by k_1 on the order of 10^{-3} to 10^{-1} s^{-1} (Tables 2 and 3) is statistically not significantly related to the specific surface area of the reactive sorbents within the three individual groups of ternary oxide reactive sorbents (Fig. 9a), nor is other single characteristics of the reactive sorbents tested. Assuming also the large value of k_1 reaction rate, that fast process is probably controlled by diffusion of the sulphur mustard from a solution toward the excess surface sites at a given reactant ratio. This assumption would explain why this fast reaction has not yet been reported by other researchers who used a different experimental design of the CWA removal, namely, mixing droplets of CWA with reactive sorbents [46] or exposing them to CWA vapours [37,45] and also by using much larger CWA load with respect to the mass of the sorbent [16]. However, MgO aerogel tested under the same experiment setup [35] as the ternary Fe–Ti–Zr oxides (Table 2) does not produce that fast reaction step, clearly indicating that the k_1 process is not only a property of our experimental design.

Both specific surface areas and acid base properties are important for the second kinetic component of Eq. (1), i.e. k_2. That rate constant is positively correlated to the content of the base functional groups on two groups of these oxides (with low and moderate Ti/Fe ratios), expressed as pH of aqueous suspension or HCl consumption to reach pH 3. Perhaps the materials performance of some of these oxides could have been improved after their alkaline treatment, similar to what was achieved by the NaOH treatment of alumina [37]. That second kinetic component is closer to the CWA degradation rate constants by the best reactive sorbents reported in previous studies (Table 3).

5. Conclusions

The obtained Fe–Ti–Zr oxides are the reactive sorbents allowing the fastest removal of sulphur mustard from a non-polar solution not having yet been reported in open literature. The use of a non-polar solvent in the degradation reaction and selection of a particular element composition of the reactive sorbents is probably essential for the very fast reaction characterised by k_1 rate constant in Table 3. The achieved half-time of sulphur mustard degradation on the order of minutes, while systems with Al and Mg oxides allow half times on the order of tens to hundred minutes under the same experimental conditions and tens of hours in the absence of solvent (see Section 1). Base functional groups on the oxides' surface enhance the rate of the second kinetic component k_2, which could be used for further tuning/improvement of these reactive sorbents. The specific surface areas of most of the sorbents tested are sufficient to achieve nearly complete (~99 percent) removal of sulphur mustard within several hours at 1/50 mass ratio to the sorbents.

Acknowledgements

The work was supported by the Academy of Sciences of the Czech Republic (Project No. AV0Z40320502) and also by the Ministry of Industry and Trade of the Czech Republic (Project No. 1HPK2/56). The authors gratefully express their thanks to S. Bakardjieva for SEM measurements, P. Bezdička for XRD measurements and P. Vorm for acid–base titrations.

References

[1] R.G. Revaiah, Chemical warfare agents–a threat to the mankind, DRDO Sci. Spectr. 1 (2009) 143–150.
[2] S.L. Bartelt-Hunt, D.R.U. Knappe, M.A. Barlaz, A Review of chemical warfare agent simulants for the study of environmental behavior, Crit. Rev. Environ. Sci. Technol. 38 (2008) 112–136.
[3] D.B. Mawhinney, J.A. Rossin, K. Gerhart, J.T. Yates, Adsorption and reaction of 2-chloro-ethyl ethyl sulfide with Al_2O_3 surfaces, Langmuir 15 (1999) 4789–4795.
[4] G.W. Wagner, P.W. Bartram, O. Koper, K.J. Klabunde, Reactions of VX, GD, and HD with nanosize MgO, J. Phys. Chem. B 103 (1999) 3225–3228.
[5] G.W. Wagner, O.B. Koper, E. Lucas, S. Decker, K.J. Klabunde, Reactions of VX, GD, and HD with nanosize CaO: autocatalytic dehydrohalogenation of HD, J. Phys. Chem. 104 (2000) 5118–5123.
[6] G.W. Wagner, L.R. Procell, R.J. O'Connor, S. Munavalli, C.L. Carnes, P.N. Kapoor, K.J. Klabunde, Reactions of VX, GB, GD, and HD with nanosize Al_2O_3. Formation of aluminophosphonates, J. Am. Chem. Soc. 123 (2001) 1636–1644.
[7] S.S. Talmage, A.P. Watson, V. Hauschild, N.B. Munro, J. Kin, Chemical warfare agent degradation and decontamination, Curr. Org. Chem. 15 (2007) 285–298.
[8] D.A. Panayotov, J.R. Morris, Catalytic degradation of a chemical warfare agent simulant: reaction mechanisms on TiO_2-supported Au nanoparticles, J. Phys. Chem. C 112 (2008) 7496–7502.
[9] D.A. Panayotov, J.R. Morris, Thermal decomposition of a chemical warfare agent simulant (DMMP) on TiO_2: adsorbate reactions with lattice oxygen as studied by infrared spectroscopy, J. Phys. Chem. C (2009) 15684–15691.
[10] T.H. Mahato, G.K. Prasad, B. Singh, J. Acharya, A.R. Srivastava, R. Vijayaraghavan, Nanocrystalline zinc oxide for the decontamintion of sarin, J. Hazard. Mater. 165 (2009) 928–932.
[11] G.K. Prasad, T.H. Mahato, B. Singh, K. Ganesan, P. Pandey, K. Sekhar, Detoxification reactions of sulphur mustard on the surface of zinc oxide nanosized rods, J. Hazard. Mater. 149 (2007) 460–464.
[12] G.K. Prasad, P.V.R.K. Ramacharyulu, K. Batra, B. Singh, A.R. Srivastava, K. Ganesan, R. Vijayaraghavan, Decontamination of Yperite using mesoporous mixed metal oxide nanocrystals, J. Hazard. Mater. 183 (2010) 847–852.
[13] T.H. Mahato, G.K. Prasad, B. Singh, A.R. Srivastava, K. Ganesan, J. Acharya, Vijayaraghavan, Reactions of sulphur mustard and sarin on V1.02O2.98 nanotubes, J. Hazard. Mater. 2–3 (2009) 1545–1549.
[14] G. K Prasad, T.H. Mahato, K. Beer Singh, P. Ganesan, K. Pandey, Sekhar, Detoxification reactions of sulphur mustard on the surface of zinc oxide nanosized rods, J. Hazard. Mater 149 (2007) 460–464.
[15] T.H. Mahato, G.K. Prasad, K. Beer Singh, K. Batra, Ganesan, Mesoporous manganese oxide nanobelts for decontamination of sarin, sulphur mustard and chloro-ethyl ethyl sulphide, Micropor. Mesopor. Mater 132 (2010) 15–21.
[16] V. Stengl, D. Kralova, F. Oplustil, T. Nemec, Manganese oxide for warfare agents degradation, under review.
[17] G.K. Prasad, T.H. Mahato, P. Pandey, M.V.S. Beer Singh, A. Suryanarayana, K. Saxena, Shekhar, Reactive sorbent based on manganese oxide nanotubes and nanosheets for the decontamination of 2-chloro-ethyl ethyl sulphide, Micropor. Mesopor. Mater. 106 (2007) 256–261.
[18] G.K. Prasad, B. Singh, K. Ganesan, Anirudh Batra, P.K. Tushar Kumeri, R. Gutch, Vijayaraghavan, Modified titania nanotubes for decontamination of sulphur mustard, J. Hazard. Mater. 167 (2009) 1192–1197.
[19] V. Stengl, S. Bakardjieva, N. Murafa, F. Oplustil, Zirconium doped titania: destruction of warfare agents and photocatalytic degradation of Orange 2, Open Process Chem. J. 1 (2008) 1–7.
[20] A. Mattsson, C. Lejon, S. Vaclav Stengl, F. Bakardjieva, P.O. Oplustil, L. Andersson, Österlund, Photodegradation of DMMP and CEES on zirconium doped titania nanoparticles, Appl. Catal. B: Environ. 92 (2009) 401–410.
[21] V. Stengl, V. Houskova, S. Bakardjieva, N. Murafa, F. Oplustil, T. Nemec, Zirconium doped nano-dispersed oxides of Fe, Al and Zn for destruction of warfare agents, Mater. Charact. 61 (2010), pp. 1080–1088.
[22] V. Stengl, J. Subrt, P. Bezdicka, M. Mariková, S. Bakardjieva, Homogeneous precipitation with urea – an easy process for making spherical hydrous metal oxides, Solid State Phenomena 90–91 (2003) 121–126.
[23] JCPDS PDF-2 database, International Centre for Diffraction Data. Newtown Square, PA, USA release 54, 2004.
[24] ICSD database, FIZ Karlsruhe, Karlsruhe, Germany, release 2011/1, 2011.
[25] S. Brunauer, P.H. Emmett, E. Teller, Adsorption of gases in multimolecular layers, J. Am. Chem. Soc. 60 (1938) 309–319.

[26] E.P. Barret, L.G. Joyner, P.P. Halenda, The Determination of pore volume and area distributions in porous substances. I. Computations from nitrogen isotherms, J. Am. Chem. Soc. 73 (1951) 373–380.
[27] V. Stengl, M. Marikova, S. Bakardjieva, J. Subrt, F. Oplustil, M. Olsanska, Reaction of HD, VX and GD with nanosized anatase TiO_2 and ferrihydrite, J. Chem. Technol. Biotechnol. 80 (2005) 754–758.
[28] J.L. Shi, J.H. GaO, Preparation of spherical zirconium salt489 particles by homogeneous precipitation, J. Mater. Sci. 30 (1995) 793–799.
[29] V.C. Farmer, Infra-red Spectra of Minerals, Mineralogical Society, London, 1974.
[30] F.F. Bentley, L.D. Smithson, A.L. Rozek, Infrared spectra and characteristic frequencies 700–300 cm^{-1}, Wiley-Interscience, New - York, 1968.
[31] S. Lowell, J.E. Shield, Powder Surface Area and Porosity, Chapman & Hall, London, 1998.
[32] J.A. de Boer, Structure & Properties of Porous Materials, Butterworths, London, 1958.
[33] G.W. Wagner, L.R. Procell, S. Munavalli, 27Al, 47,49Ti, 31P, and 13C MAS NMR study of VX, GD, and HD reactions with nanosize Al2O3, conventional Al2O3 and TiO2, and aluminum and titanium metal, J. Phys. Chem. C 111 (2007) 17564–17569.
[34] G.K. Prasad, Decontamination of 2-chloro-ethyl phenyl sulphide using mixed metal oxide nanocrystals, J. Sci. Ind. Res. 69 (2010) 835–840.
[35] V. Stengl, S. Bakardjieva, M. Marikova, J. Subrt, F. Oplustil, M. Olsanská, Aerogel nanoscale magnesium oxides as a destructive sorbent for toxic chemical agents, Cent. Eur. J. Chem. 2 (2004) 16–33.
[36] F. Oplustil, T. Nemec, M. Olsanska, Nanodispersive oxides and hydroxides Ti, Fe, Al, Zn and Zr for warfare agents decontamination, Research report Military Technical Institute of Protection Brno, Czech Rep. (2009), pp. 1–24.
[37] H. Tang, Z. Cheng, H. Zhu, G. Zuo, M. Zhang, Effect of acid and base sites on the degradation of sulfur mustard over several typical oxides, Appl. Catal. B: Environ. 8 (2008) 323–333.
[38] W. Creasy, R. Fry, D. McGarvey, D. Hendrickson, H.D. Durst, Methods for chemical warfare agent reaction studies on reactive films using headspace GC/MS and high resolution magic angle spinning (HRMAS) NMR, Main Group Chem. 3–4 (2010), 1745–1167.
[39] K.J. Klabunde, J. Stark, O. Koper, C. Mohs, D.G. Park, S. Decker, Y. Jiang, I. Lagadic, D.J. Zhang, Nanocrystals as stoichiometric reagents with unique surface chemistry, J. Phys. Chem. 100 (1996) 12142–12153.
[40] A.V. Vorontsov, L. Davydov, E.P. Reddy, C. Lion, E.N. Savinov, P.G. Smirniotis, Routes of photocatalytic destruction of chemical warfare agent simulants, New J. Chem. 26 (2002) 732–744.
[41] T. Hirakawa, N. Mera, T. Sano, N. Negishi, K. Takeuchi, Decontamination of chemical warfare agents by photocatalysis, Yakugaku Zasshi-J. Pharm. Soc. Jpn. 129 (2009) 71–92.
[42] G.K. Prasad, T.H. Mahato, B. Singh, P. Pandey, A.N. Rao, K. Ganesan, R. Vijayraghavan, Decontamination of sulfur mustard on manganese oxide nanostructures, AIChE J. 53 (2006) 1562–1567.
[43] A. Saxena, B. Singh, A.K. Srivastava, M.V.S. Suryanarayana, K. Ganesan, R. Vijayaraghavan, K.K. Dwivedi, Al2O3 nanoparticles with and without polyoxometalates as reactive sorbents for the removal of sulphur mustard, Micropor. Mesopor. Mater. 3 (1998) 364–375.
[44] A. Saxena, A. Sharma, A.K. Srivastava, B. Singh, P.K. Gutch, R.P. Semwal, Kinetics of adsorption of sulfur mustard on Al2O3 nanoparticles with and without impregnants, J. Chem.Technol. Biotechnol. 84 (2009) 1860–1872.
[45] M. Winter, D. Hamal, X. Yang, H. Kwen, S. David Jones, K.J. Rajagopalan, Klabunde, Defining reactivity of solid sorbents: what is the most appropriate metric? Chem. Mater. 21 (2009) 2367–2374.
[46] H. Tang, Z. Cheng, L. Zhou, G. Zuo, L. Kong, Degradation of sulfur mustard and sarin over hardened cement paste, Environ. Sci. Technol. 43 (2009) 1553–1558.
[47] O. Danek, V. Stengl, S. Bakardjieva, N. Murafa, A. Kalendova, F. Oplustil, Nanodispersive mixed oxides for destruction of warfare agents prepared by homogeneous hydrolysis with urea, J. Phys. Chem. Solids 68 (2007) 707–711.
[48] F. Oplustil, T. Nemec, M. Olsanska, Realization of new nanostructures from nanodispersive oxido-sulphides Ti, Cd, Zn as active materials for the degradation of warfare agents,Research report Military Technical Institute of Protection Brno, Czech Rep. (2009), pp. 1–21.
[49] F. Oplustil, T. Nemec, M. Olsanska, Realization of new nanostructures from nanodispersive oxido-sulphides Ti, Cd, Zn as active materials for the degradation of warfare agents, Research report of Military Technical Institute of Protection Brno, Czech Rep. (2010), pp. 1–55.